THE JOURNAL OF PHYSICAL CHEMISTRY A

ARTICLE

pubs.acs.org/JPCA

Single and Multi-Exciton Dynamics in Aqueous Protochlorophyllide Aggregates

Olga A. Sytina,* Ivo H. M. van Stokkum,† Rienk van Grondelle,† and Marie Louise Groot†

Department of Physics and Astronomy, Faculty of Sciences, Vrije Universiteit, De Boelelaan 1081, 1081 HV Amsterdam, The Netherlands

Supporting Information

ABSTRACT: In plants, the oxidoreductase enzyme POR reduces protochlorophyllide (Pchlide) into chlorophyllide (Chlide), using NADPH as a cofactor. The reduction involves the transfer of two electrons and two protons to the C17═C18 double bond of Pchlide, and the reaction is initiated by the absorption of light by Pchlide itself. In this work we have studied the excited state dynamics of Pchlide dissolved in water, where it forms excitonically coupled aggregates, by ultrafast time-resolved transient absorption and fluorescence experiments performed in the 480−720 nm visible region and in the 1780−1590 cm^{-1} mid-IR region. The ground state visible absorption spectrum of aqueous Pchlide red shifts and broadens in comparison to the spectrum of monomeric Pchlide in organic solvents. The population of the one-exciton state occurs at low excitation densities, of <1 photon per aggregate. We characterized the multiexciton manifolds spectra by measuring the absorption difference spectra at increasingly higher photon densities. The multiexciton states are characterized by blue-shifted stimulated emission and red-shifted excited state absorption in comparison to those of the one-exciton manifold. The relaxation dynamics of the multiexciton manifolds into the one-exciton manifold is found to occur in ∼10 ps. This surprisingly slow rate we suggest is due to the intrinsic charge transfer character of the PChlide excited state that leads to solvation, stabilizing the CT state, and subsequent charge recombination, which limits the exciton relaxation.

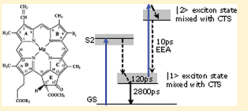

INTRODUCTION

Protochlorophyllide (Pchlide) is a natural porphyrin, a precursor of chlorophyll *a* that is synthesized by plants for its photosynthetic apparatus. In plants, the oxidoreductase enzyme POR reduces protochlorophyllide into chlorophyllide, using NADPH as a cofactor. The reduction involves the transfer of two electrons and two protons to the C17═C18 double bond of Pchlide, and the reaction is initiated by the absorption of light by Pchlide itself.[1,2] To fully determine the catalytic mechanism, an understanding of the intrinsic photochemistry of PChlide is required. Earlier, our and other groups studied the photochemistry of monomeric PChlide in organic solvents, both experimentally and theoretically.[3−7] A time-dependent density functional theory study by Zhao et al.[8] indicated that the Pchlide excited state has significant internal charge-transfer character. Experimentally, upon formation of the excited state, a dynamic red shift and quenching of emission is observed, not related to population decay,[6] which shows that this CT state is stabilized by solvation and, in the case of protic solvents, the dynamic strengthening of H-bond interactions. This reactivity of the PChlide molecule is likely the driving force for the catalytic reaction.

PChlide binds to the POR enzyme in a monomeric form, as its absorption spectrum when bound to the enzyme resembles that of PChlide in MeOH.[6,9,10] However, red-absorbing aggregates of Pchlide have been observed in in vivo studies, in etiolated leaves (see, for a detailed review of the POR in vivo studies, Belyeva and Litvin[11]), but their role in the catalytic mechanism has remained unclear so far. Here, we study the excited state properties of PChlide dissolved in water, where it self-aggregates in complexes in which the Pchlide molecules experience significant excitonic coupling. Self-aggregation of porphyrins and their analogues affect the optical absorption and emission properties. Generally, when two identical molecules come in close proximity of each other, their interacting transition dipole moments create a system of coupled electronic transitions. This so-called exciton coupling is in the case of porhyrins facilitated by the conjugated electron system via $\pi-\pi$ stacking. Excitonic coupling causes a splitting of the electronic energy levels of individual molecules into a manifold of excitonic levels. So-called H-aggregates, in which two adjacent molecules are stacked on top of each other, show a blue shift of the electronic absorption relatively to the monomer absorption band, whereas *J*-aggregates in which neighboring molecules are oriented in line demonstrate a red shift in the electronic absorption spectra.[12,13]

Chlorophyll *a* displays a clear change in its absorption and emission spectrum when it is put in aqueous solution: the Q_Y band experiences a dramatic shift from 663 to 747 nm and the yield of chlorophyll fluorescence in wet organic solution is found to be inversely proportional to the molar fraction of water.[14,15] The alteration of the optical properties of chlorophyll in aqueous solution is due to the formation of aggregates and chlorophyll−water

Special Issue: Graham R. Fleming Festschrift

Received: September 1, 2010
Revised: November 15, 2010
Published: December 20, 2010

adduct states, and the resulting excitonic interactions within the aggregate. Early on, (bacterio)chlorophyll aggregates have been investigated both experimentally and theoretically, because of their relevance to the organization of the pigments that constitute the electron donors in reaction center proteins of photosynthetic bacteria and green plants in Photosystem I,[15−18] and for the organization of the bacteriochlorophyll pigments in chlorosomes.[19,20] For chlorophyll−water aggregates, polarized spectroscopy and neutron diffraction suggested a long tube-like structure of the aggregates.[21,22] Applying quantum chemical calculations to a chlorophyll−-water aggregate, Linnanto et al.[22] modeled a helical structure with a circular diameter of 12 nm, close to the experimentally observed by neutron diffraction diameter of 11.4 nm of the aggregates in solution. Typically, the aggregates consisted of repeating tetramers. No ultrafast time-resolved spectroscopy on chlorophyll *a* in aqueous solution has been performed to characterize the dynamics within these aggregates, apart from the work of Helenius et al.,[23,24] who measured single-color transient absorption changes. In this work we present the results of ultrafast time-resolved transient absorption and fluorescence experiments performed on protochlorophyllide in aqueous solution in the 480−720 nm visible region and in the 1780−1590 cm^{-1} mid-IR region. Our spectra show the population of multiexciton manifolds at increased photon densities, probably up to $n = 4$. The relaxation from the multiexciton to the single exciton state is unexpectedly slow and occurs in about 10 ps. We conclude from our results that both excitonic interactions and charge transfer solvation processes, via increased H-bonding interaction, determine the steady-state and dynamical optical properties of Pchlide in aqueous solution.

MATERIALS AND METHODS

Protochlorophyllide was extracted from *Rhodobacter capsulatus* ZY5 as is described previously by Heyes[9] and was dissolved in neat H_2O or D_2O (purchased from Merck) to an OD of ∼0.2 at 650 nm in a 200 μm cell.

Visible transient absorption measurements were performed by pumping the red edge of the Soret transition of Pchlide at 475 nm with a 85 fs laser pulse, and monitoring the resulting absorption changes in the region of the Q_X and Q_Y electronic transitions by a 480−720 nm white-light probe beam. After passing the sample cell, the probe beam was dispersed in a 2 nm resolution spectrograph and imaged on to a 256 element diode array. The instrument response function of the setup was about 120 fs, and the experiments were performed at a 1 kHz repetition rate. Transient absorption mid-IR spectra were measured on the same setup (described in more detail in refs 25 and 26) in the 1580−1800 cm^{-1} region using 400 nm excitation. In both experiments the pump beam was sent over a moveable delay line, enabling the measurement of absorption difference spectra at time delays from −15 ps to +5.5 ns. The excitation energy per pulse was adjusted by a neutral density filter to between 10 nJ up to 430 nJ in the vis−vis experiments, and 500 nJ in the mid-IR−vis experiment and focused into a 160 μm diameter spot.

Time-resolved fluorescence was collected in the region 450−750 nm using a synchroscan streak camera Hamamatsu C5680, upon 400 nm excitation with a 50 fs laser pulse at a 250 kHz repetition rate, with a setup described in more detail by van Stokkum et al.[27] The instrument-response function of this setup was estimated to be ∼3.5 ps for measurements performed in a 200 ps time window. The excitation energy in the experiment was 1 nJ per laser pulse.

In every experiment the relative polarizations of the pump and probe light were oriented at the magic angle (54.7°). For the time-resolved fluorescence measurements a stirred 1 cm quartz cell was used, for the time-resolved transient absorption measurements a 200 μm path cell was used, with CaF_2 windows. The latter was built into a Lissajous sample scanner which allowed to collect the signal from a fresh sample spot for each laser shot.

Steady-state visible absorption spectra were recorded using a Perkin-Elmer Lambda 40UV/VIS spectrograph, steady-state fluorescence spectra were collected by a Fluorolog FL-1039 apparatus, upon excitation at 400 nm through a 1 nm wide filter.

The fitting methods are described in more detail in van Stokkum et al.[27] Briefly, the time-resolved data both in the visible and in the mid-IR regions were fitted globally with a minimal sum of exponentially decaying components. Here, we use sequential models to describe the time-dependent evolution of the transient data with minimal bias for a physical model.

RESULTS

Steady-State Absorption and Emission Spectra. Absorption and fluorescence emission spectra of Pchlide dissolved in 100% H_2O are depicted in Figure 1A. The positions of the S2←S0 and S1← S0 absorption bands of Pchlide in neat water are significantly red-shifted in comparison to Pchlide in an organic solvent like THF. In aqueous solution the Q_Y maximum is located between 650 and 654 nm with fwhm ∼40 nm, depending on the Pchlide concentration, whereas in THF it is at 629 nm and fwhm ∼23 nm. In the Soret region, the position of the main peak shifts from 444 to 480 nm. The emission spectrum of Pchlide in H_2O has a badly defined shape and basically consists of a broad signal extending from 600 to 700 nm with a peak at 650−660 nm. The intensity of the fluorescence emission is about 300 times weaker than that of Pchlide in organic solvents. We observed no difference between the steady-state absorption spectra of Pchlide in H_2O and D_2O, besides minor variation in peak positions, which mainly depend on the concentration of the pigment in a particular sample preparation.

Addition of a few droplets of pyridine or THF into the Pchlide aqueous solution leads to a gain and blue shift of the Q_Y emission intensity. With a deconvolution analysis of the Q_Y absorption band of the water−pyridine−Pchlide and water−THF−Pchlide mixtures, we could disentangle a red and a blue population (Figure 1B,C).

The blue states are typical for dry solutions, whereas the red states are characteristic for wet solutions. However, the red 646 nm state found in the water−Pchlide−THF mixture can also be generated in dry THF upon increase of the pigment concentration. Figure 1D demonstrates how a change in the relative concentration of THF solvent and Pchlide affects the steady-state spectrum. A typical low concentration spectrum of Pchlide dissolved in THF has peaks at 441 and 629 nm; increasing the Pchlide concentration leads to the appearance of new bands at 420, 475, 446, and 646 nm. The positions of the new bands in the Soret are similar to those found in aqueous solutions. We also noted that a further 2 nm shift of the Q_Y absorption band toward the red can be forced by addition of base to the Pchlide water solution, i.e., with increase of OH^- concentration.

The significant red shifts of the absorption and emission spectra are indicative for the formation of aggregates of Pchlide, as similar effects have been observed for chlorophyll aggregates in H_2O and have been shown to be due to excitonic interactions.[14,21,28,29]

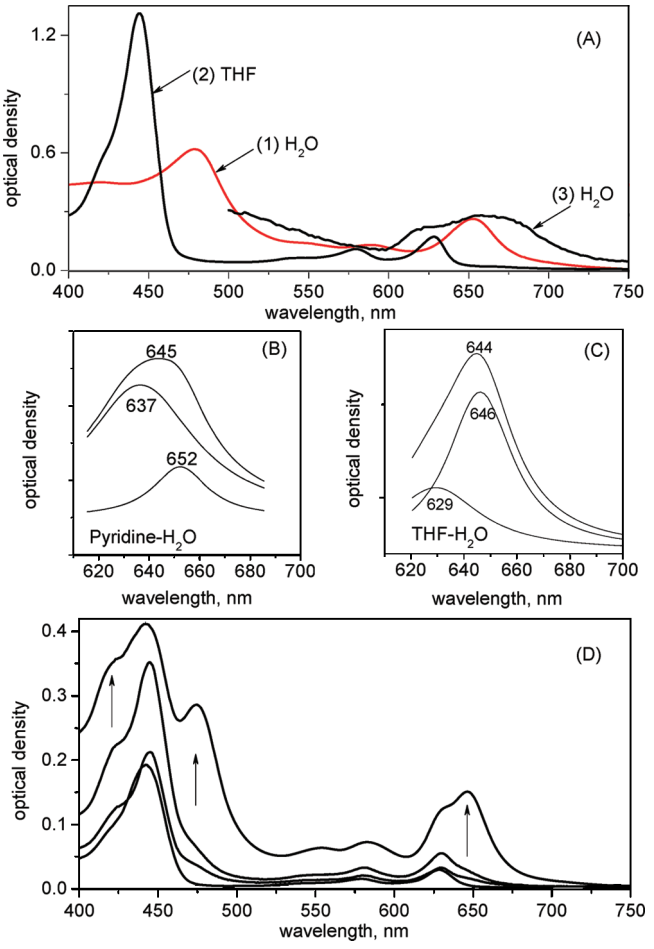

Figure 1. Absorption and emission spectra of Pchlide. (A) 1, Pchlide absorption in 100% neat water solution recorded in a 1 cm cuvette; 2, Pchlide absorption in THF; 3, normalized steady-state fluorescence emission of PChlide in 100% neat water upon 400 nm excitation. (B) Lorentzian deconvolution (lower two curves) of the Q_Y absorption band of Pchlide in H_2O containing a few droplets of pyridine (top curve) and (C) the same as (B), for PChlide in THF. (D) Pchlide absorption spectra in THF recorded in 200 μm CaF_2 cell at increased concentration of pigment. New bands appearing upon concentration increase are indicated by arrows.

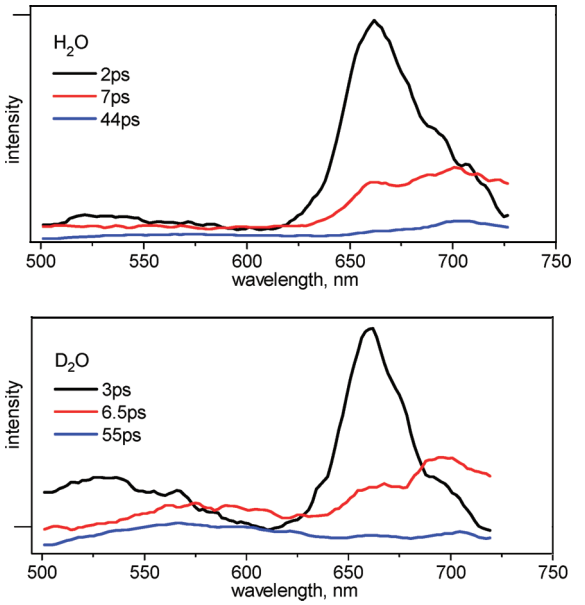

Figure 2. EAS resulting from global analysis of the time-resolved fluorescence of Pchlide in H_2O (top panel) and Pchlide in D_2O (bottom panel) recorded upon excitation with 1 nJ laser pulses at 400 nm.

Also, our observations of reversible loss of Pchlide emission depending on solvent composition, are similar to observations reported for chlorophyll in water mixtures[14] and for Pchlide in aqueous methanol.[30]

Time-Resolved Fluorescence. Time-resolved fluorescence traces of Pchlide in H_2O and D_2O were collected in the 500−750 nm region, in a 200 ps time window (Figure S1, Supporting Information). The traces were analyzed globally[31] with a sum of three sequentially decaying components. The result is shown in Figure 2 in the form of evolution-associated spectra (EAS). The first EAS represents the spectrum appearing directly after excitation and has a main peak around 660 nm. After 2 ps, the intensity of the main band at 660 nm significantly diminishes, but there is a small gain of signal above 700 nm. This results in a double-peaked spectrum with a stronger emission at 690 nm rather than at 660 nm. A further decay of emission occurs at 7 ps and ~50 ps. The final spectrum with the 50 ps lifetime has a very badly defined shape because of its low intensity. The differences in emission spectra and lifetimes between H_2O and D_2O are likely due to slightly varying sample concentrations. The observed dynamics are dramatically different from those described previously for Pchlide in organic solvents, where a set of varying lifetimes on the subpicosecond, picosecond, and nanosecond lifetimes was reported.[32] Here, in water, the Pchlide fluorescence emission is virtually all quenched on a 2−7 ps time scale, and in conjunction with quenching, the emission shifts to lower energy. The latter may represent transfer of the excitation to sites of lower energy within an aggregate, or solvation processes.

Transient Absorption Spectra. To determine whether the emission is quenched due to a loss of excited states, or due to the formation of a nonradiative product, we performed transient absorption difference measurements. In addition, to test a possible power dependence of the kinetics, several excitation densities ranging from 10 to 430 nJ per pulse were used.

All data sets were fitted globally with a sum of four sequentially decaying components. The evolution associated difference spectra of each kinetic component (EADS), and the lifetimes, for each excitation energy, are shown in Figure 3 and in Table 1 of the Supporting Information. The quality of the global fit can be visually judged in Figure 4. The kinetics show a pronounced dependence on excitation density: the first lifetime is subpicosecond, ~0.5−0.6 ps; the second lifetime increases from ~2.3 to 8 ps with increasing density; the third lifetime increases from 60 to 150 ps and the last increases from 1.5 ns to 3−4 ns. Negative bands in the corresponding EADS in Figure 3 represent bleach of the ground state absorption and stimulated emission (SE); positive bands correspond to absorption from the excited state to higher lying electronic levels (ESA).

Low Excitation Energy. Similar to the fluorescence decay dynamics, the transient absorption (TA) dynamics demonstrate an ultrafast decay of broad difference signals. Comparing the 10 nJ TA dynamics with the fluorescence emission dynamics, which were recorded with an excitation energy of 1 nJ per pulse, we see that in the TA about half of the signal is retained after ~2.3 ps, but the fluorescence emission virtually all decays on this time scale. This indicates that the initial loss of emission signal is not due to a loss of excited states, but to a reduction of the radiative

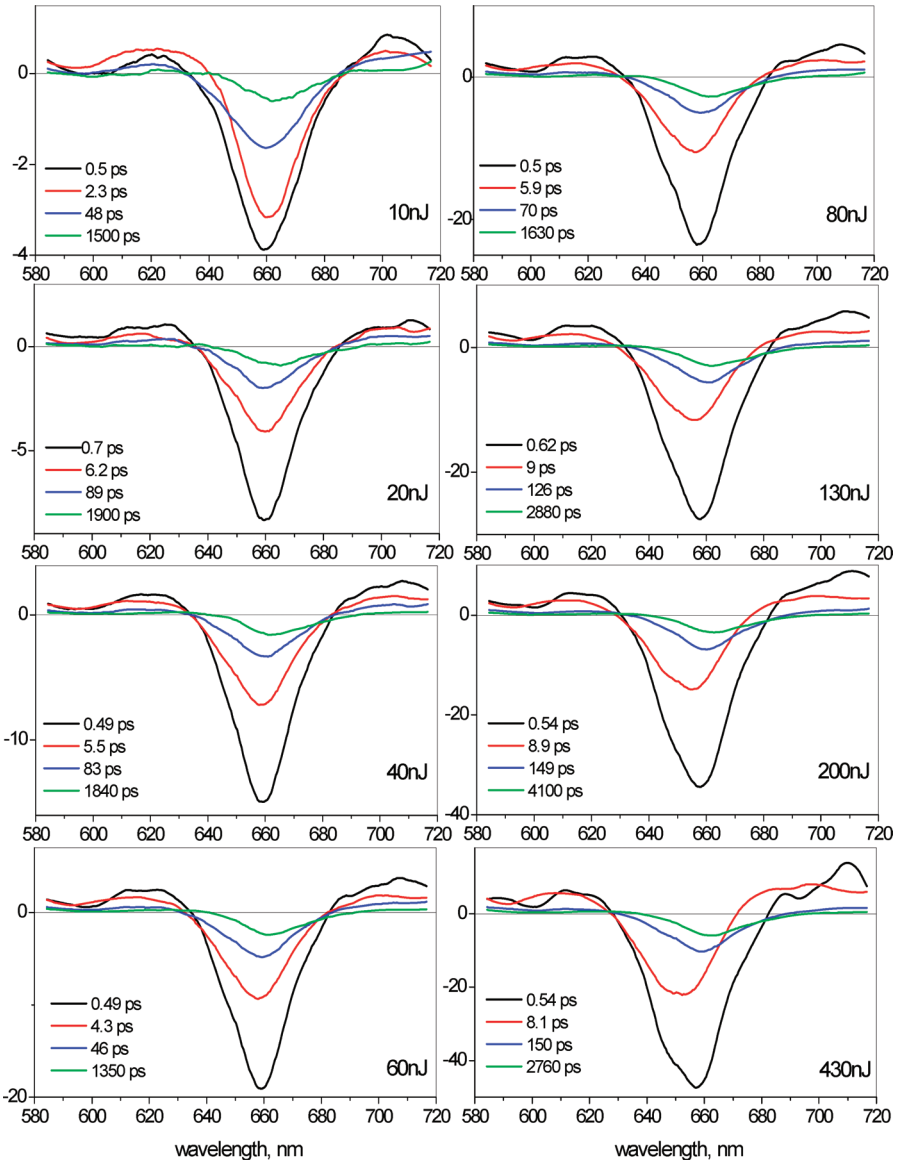

Figure 3. EADS resulting from global analysis of TA data of Pchlide in D_2O excited at 475 nm with powers of 10, 20, 40, 60, 80, 130, 200, and 430 nJ per laser pulse.

rate, due to the formation of a "product" state with no or low transition dipole moment. Notably, as in the fluorescence experiment, this process occurs in conjunction with transfer of the excitation to sites of lower energy, since the pump−probe data show relatively more loss of blue signal, between 640 and 660 nm. A further ∼45% loss of the signal occurs with a time constant of 48 ps, in conjunction with a clear decay at the blue side of the difference spectrum, though no obvious shift in the 660 nm peak is observed.

High Excitation Energy. At excitation pulse energies above 20 nJ, the amplitude of the initial decay increases: about half of the initial negative signal at 660 nm is lost after 0.5−0.7 ps (black to red evolution in Figure 3). In addition, the first EADS show increased intensity at the high energy side, around 640−645 nm, with increasing pulse energy. This process goes along with a transition from negative to positive amplitudes in the 670−680 nm region. A comparison of selected time traces recorded with 20 and 430 nJ illustrates this spectral change in Figure 4. One can clearly see the dramatic difference in kinetics between the traces recorded at 644 and 675 nm, whereas the dynamics of the signals at 660 nm seem to be less affected upon 20-fold power increase. As we will show below, this is a consequence of putting more than one excitation in the Pchlide aggregate, which leads to the population of the two-, three- or higher-exciton manifolds, that apparently have different spectral features than the one-exciton manifold. Examination of the amplitudes of the TA signals at $t = 0$ ps (black spectrum) reveals pronounced power-dependent saturation behavior.

Saturation of the Transient Absorption Signals. The saturation behavior of the TA signals of PChlide in water is visualized in Figure 5A. We compare the saturation of PChlide in water with that of PChlide in organic solvent, for which we assume PChlide to be in monomeric form.[32] The TA saturation curves in neat water explicitly demonstrate a nonlinear behavior, whereas the curves obtained in organic solvents show linear-like dependence on excitation power within the whole range of powers. The observed

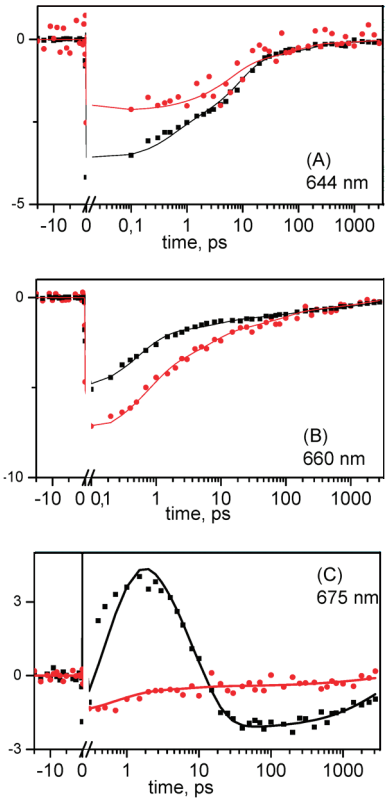

Figure 4. Traces of transient absorption of Pchlide in D_2O. Solid lines represent the fit, red circles are data points recorded with 20 nJ, and black squares are data points recorded with 430 nJ excitation energy per pulse: (A) 430 nJ trace at 644 nm normalized to the amplitude of the 20 nJ signal at 1 ns delay; (B) 430 nJ trace at 660 nm normalized to the amplitude of the 20 nJ signal at 1 ns delay; (C) 675 nm traces without normalization. The misfit at early times in the high power experiment is because of a contribution of a nonlinear artifact to the signal. In the global analysis an additional component was included to fit this dynamics; however, a perfect fit is difficult to achieve, and therefore the dynamics at −200 to +200 fs was ignored.

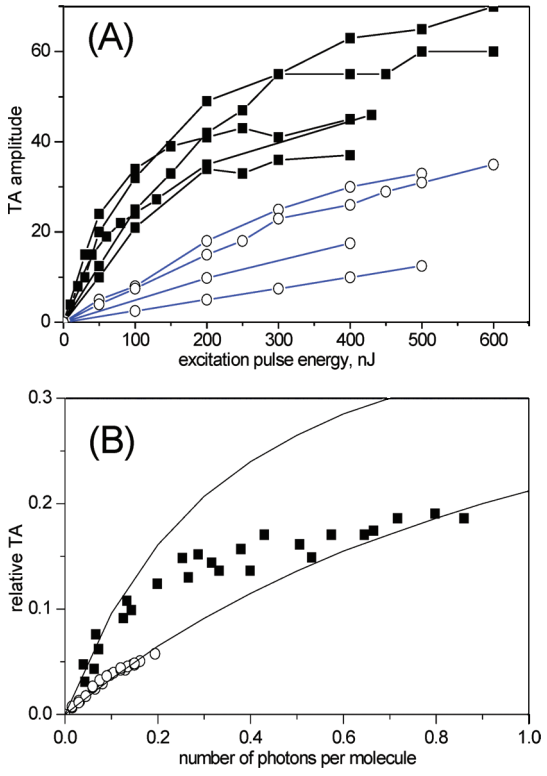

Figure 5. (A) Saturation of the transient absorption of Pchlide in H_2O and D_2O (black dots) and in organic solvents methanol and THF (blue dots) as a function of excitation energy. (B) Corrected saturation curve of Pchlide TA in water and organic solvents. The black squares are the experimental data averaged over five samples (three in D_2O and 2 in H_2O), the open circles are experimental data averaged over four samples in THF and methanol. The lines are saturation functions[33] fitted to the experimental data with number of photons per molecule $n=1$ for organic solvents and $n = 1/3.5$ for water.

variation in amplitudes of the TA signals is due to variations in the concentration of PChlide among different samples. This scatter can be partly eliminated if the *Y*-scales of each data set are converted into a relative change in absorption, thus making the experimental data independent of the sample preparation and variation of concentrations. For this purpose the integrated bleached difference absorption signals at $t = 300$ fs were normalized to the integrated absorption of the Q_Y band of each sample multiplied by factor 2 that accounts for 50% contribution of SE to the bleached signal, and the *x*-scale was converted to number of photons per molecule, as detailed in the Supporting Information.

The experimental saturation curves can be fitted by the function derived in Groot et al.[33] for saturation of a TA signal of a two-level system in a polarized experiment:

$$N = \frac{1}{2}(1 - e^{-2n(\theta)})$$

where N is the fraction of aggregates in the excited state, $n(\theta)$ is the number of absorbed photons per aggregate, θ is the angle between the (vertically polarized) exciting laser pulse and the transition dipole of the pigment.

The data in organic solvents can be best fitted with the saturation rate $n = 1$ photon/molecule (Figure 5B), confirming the monomeric state of PChlide. However, for the aqueous data only the initial linear part can be fitted, with saturation rate $n = 1/3.5$ photons/molecules. The deviation between data and fit at higher excitation densities shows that although fewer photons are required to start saturation of the TA signal for aqueous PChlide than for PChlide in organic solvent, putting in *more* photons does not lead to the full 50% bleaching of the absorption signal (note that stimulated emission process prevents 100% bleach), as would be expected for a simple two-level system.

Describing the TA Dynamics in a Target Model. From the time-dependent absorption saturation measurements and their global analysis it is clear that the dynamics of Pchlide in aqueous solution demonstrates pronounced nonlinear dependence on power. We disentangled the low-power and high-power contributions by applying a target analysis to the data, with the kinetic scheme shown in Figure 6. In this scheme the low-power dynamics is represented by the sequential formation in time of four states (1, 2, 3, 4). To account for the high-power dynamics, we introduced an additional pathway, with two compartments 5 and 6. In the analysis both states 1 and 5 can be excited by the laser pulse, and their relative populations are free fitting parameters. Also, in parallel, there is a contribution of a coherent artifact. We assume that the high-power states 5 and 6 describe the populations of the multiexcitation manifold and that this relaxes/annihilates either to the GS or to the one-excitation

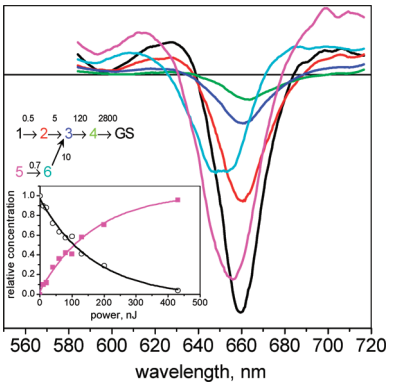

Figure 6. Species-associated difference spectra obtained from simultaneous fitting of transient absorption difference spectra recorded in solution of Pchlide in D_2O at different excitation powers against the indicated target model. The model consisted of the sequentially decaying compartments 1, 2, 3, and 4, with compartments 5 and 6 decaying into compartment 3. The fitted time constants are indicated in picoseconds. Color coding of the spectra matches those of the compartments. (Inset) relative concentrations of state 1 (one exciton) and state 5 (multiexciton state) as a function of excitation power, as deduced from the fitting against the target model.

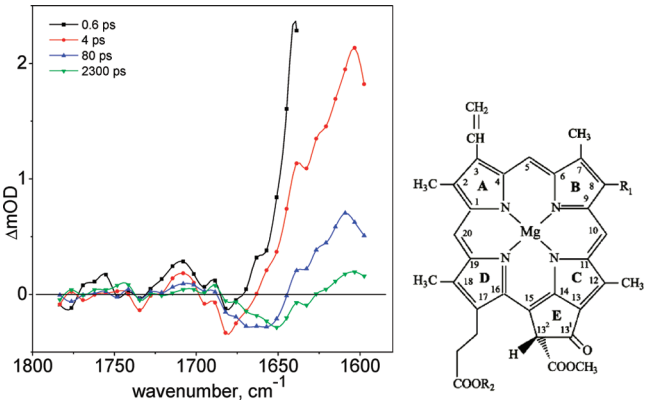

Figure 7. EADS of time-resolved mid-IR transient absorption of Pchlide in D_2O upon 400 nm excitation.

manifold because in the global analysis the major power-dependent spectral difference is observed in the first and second EADS. Therefore, the most probable kinetic scheme should include a decay of compartment 6 either to states 3 or 4, or directly to the ground state, in ~10 ps after excitation. With this model we fitted the whole data set consisting of 9 individual measurements at different excitation energies ranging from 10 to 430 nJ per pulse simultaneously, and species-associated difference spectra (SADS) of each compartment, as well as their lifetimes and relative populations of the two schemes to the overall signal amplitude were estimated. The result of the target analysis and the kinetic scheme are depicted in Figure 6.

We see that upon increasing excitation density, the population of compartment 5 increases, and the population of compartment 1 decreases, resulting in the 5 → 6 → 3 → 4 → GS kinetic scheme dominating at high excitation energies (inset in Figure 6). The contribution of the coherent artifact was negligible after 0.2 ps and did not significantly affect the target analysis results. It appeared that the best separation of "blue" and "red" states was achieved in a model where the population of the nonlinear branch 5−6 decays into compartment 3 in the sequential scheme. When it decayed to the GS, a considerable portion of blue amplitudes was still present in the black and red spectra (not shown).

The evolution in the low-power compartments, loss of signal accompanied by a red shift of the signal, occurs with lifetimes of 0.5 ps, 5 ps, 120 ps, and 2.8 ns. Only 10% of the initial amplitude is left in the final 2.8 ns spectrum, and the bleaching maximum has shifted from 659 nm to 663−664 nm. The initial spectrum 5 of the high-power dynamics peaks at 656 nm and has a lifetime of 0.7 ps. The next spectrum, 6, has a lifetime of 10 ps and a broadened double-peaked shape in the 650 nm region.

The signal between 670 and 720 nm signal is positive and flat; in this region there is a distinct power-dependent transition from negative to positive amplitudes together with gain in the blue side of Q_Y bleach (see the 675-nm time trace in figure 4.C).

Time-Resolved Mid-IR Spectroscopy. Transient absorption spectra between 1780 and 1660 cm^{-1}, in the region of the C═O 13^1 keto and 13^2 ester vibrations of PChlide in neat D_2O, were collected to investigate the influence of H-bonding and aggregation behavior on the PChlide excited state dynamics. In the mid-IR TA experiment a sample with an optical density similar to the one used in the visible experiments, i.e., about 0.2 at 650 nm, was excited in the Soret band at 400 nm, with a laser power of ~500 nJ per pulse, which corresponds to the saturating regime. The time-resolved data were globally best fitted with a sum of four sequentially decaying exponential components of 0.6 ps, 4 ps, 80 ps, and 2.3 ns. The corresponding evolution associated difference spectra (EADS) are shown in Figure 7. The lifetimes obtained in the global analysis of the mid-IR TA data are similar to the ones found for the visible TA data, at high power. Therefore, the final long-lived spectrum in the visible region can be associated with the final spectrum in the mid-IR region.

The EADS of Pchlide in D_2O display multiple negative bands, presumably belonging to the GS C^{13}═O keto stretching vibrations, apart from that at 1734 cm^{-1}, which can be assigned to the GS-ester mode.

The mid-IR spectra and dynamics observed in neat D_2O are remarkably different from those observed in the aprotic solvent THF.[6] In THF, where PChlide is monomeric and non-H-bonded, the spectrum showed only a single keto band, at 1708 cm^{-1}, which downshifted to 1660 cm^{-1} in the excited state, and the position of the ester mode was found at 1750 cm^{-1} in the GS and at 1738 cm^{-1} in the excited state.[6] In the protic solvents methanol and water buffer solution, two bleached ground state keto bands, due to two subpopulations of pigments, were observed.[6] Here, in neat D_2O multiple, broad negative bands are observed: the initial spectrum displays a bleached ground state band at 1680 cm^{-1}, a broad extremely intense positive light-induced band in the region below 1670 cm^{-1}, a small negative band at 1734 cm^{-1}, and positive signal between 1715 and 1690 cm^{-1}. The positive signal below 1670 cm^{-1} decays for a large part and red shifts in 0.6 ps, in conjunction with decay of the positive signal at 1704 cm^{-1} (1st and second EADS in figure 7). The loss of the major part of the positive signal below 1670 cm^{-1} is accompanied by the appearance of negative bands at ~1666 and 1650 cm^{-1}. In 4 ps the initially bleached bands at 1694 and 1680 cm^{-1} recover and additional negative signals at 1650 and 1634 cm^{-1} appear. The present observation of a range of downshifted Pchlide keto frequencies in neat water is an indication of the existence of several subpopulations of C═O keto groups with varying hydrogen bond strengths, formed either between subunits of an aggregate or with the surrounding solvent. The data do not

allow us to make a distinction between specific H-bonds in Pchlide aggregates, and for that further investigation is required. However, it is clear that the H-bonding interactions in Pchlide aggregates are as strong as when Pchlide is bound to the POR enzyme, since the keto carbonyl of Pchlide in POR is located at 1653 cm^{-1}.[34]

DISCUSSION

In this work we have used time-resolved visible and mid-IR spectroscopy to study aggregates of PChlide in neat water. We find that the PChlide aggregates are characterized by broadening and red shift of the steady-state absorption and a low steady-state emission signal. The significant red shifts of the absorption and emission spectra are indicative of the formation of aggregates of Pchlide, as similar effects have been observed for chlorophyll aggregates in H_2O that have been shown to be due to excitonic and charge transfer interactions.[14,21,28,29] Also the observation of reversible loss of Pchlide emission depending on solvent composition is similar to observations reported for chlorophyll in water mixtures[14] and for Pchlide in aqueous methanol.[30]

The time-resolved experiments show that loss of emission occurs with time constants of 3, 7, and 50 ps, and consistent with that, at low excitation density the dynamics in the transient absorption experiments in the visible occur in 0.5 ps, 2.3 ps, 48 ps, and 1.5 ns. At saturating excitation density these dynamics change into 0.5 ps, 8 ps, 150 ps, and 2.8 ns, which is similar to the dynamics in the mid-IR spectral region (0.6 ps, 4 ps, 80 ps, 2.3 ns). We applied a kinetic model to the visible TA data to disentangle spectral features and dynamics typical for low excitation power and of high excitation power. In the following we will discuss the different aspects of these dynamics and their relation to the structural organization of Pchlide in aggregates in more detail. Here, we will qualitatively take into account that according to exciton theory, when N monomers form an aggregate, the excited states are split into N excitonic manifolds, each containing certain number of sublevels.[35] Upon absorption of one photon, the aggregate is promoted into the one-exciton state; with two, three, and four photons it can be promoted to correspondingly higher exciton manifolds.

Exciton Dynamics in Pchlide Aggregates. The TA signals of Pchlide in water saturate at lower excitation densities than of PChlide in THF or methanol. From the different rates of saturation of 1/3.5 and 1 photons/PChlide, respectively, we estimate the average aggregate size to be ~3−4. However, this is likely a lower estimate of the average aggregate size, since we used the net absorption difference signal at 0.3 ps delay time, and some quenching of emission may have occurred already at that time. This aggregate size is similar to a minimal estimate for chlorophyll *a* in water $(\text{Chl a-}H_2O)_n$ adduct states where long rod-like and helix-like structures consisted of repeating tetramers have been computed by Linnanto et al.[22]

The deviation of the saturation curve of the PChlide aggregates at higher excitation energies from the saturation curve expected for a simple two-level system may be due to a reduced chance of absorption of a second photon in an aggregate, if having one excitation in the aggregate leads to reduced absorption at the wavelength of excitation (475 nm). However, a more important effect appears to be that in the multiexciton spectra the net signals of bleaching of the ground state absorption, stimulated emission and induced absorption are not so different in size from the single-exciton spectra. At the higher excitation densities, the transient spectra do show clearly different spectral features and are therefore indicative of the population of multiexciton levels: additional negative and positive signals appear both at the high energy and the low energy side of the main band, respectively. Applying the target model depicted in Figure 6, we could disentangle the low excitation energy and high-excitation energy dynamics and SADS. The low energy spectra and dynamics correspond to the dynamics within the one-exciton manifold, but the high-energy dynamics and SADS should be interpreted taking into consideration the multiexciton manifold electronic transitions. The relative fractions show that at the highest excitation density, dominantly multiexciton levels are populated.

As an illustration of the special spectral signature of the multiexciton manifold, let us assume that putting more photons into an aggregate induces correspondingly larger signals, which after annihilation processes result in the survival of one excitation per aggregate. Then this should result into a ratio of initial- to final- spectral area that is larger for the high-excitation energy case, than for the low-energy case. In contrast, we find a ratio of 99/14 = 7 for the 10 nJ and 1317/155 = 8.5 for the 430 nJ case. This illustrates the premise that more photons per complex results in larger signals is largely wrong. Inspection of the SADS in Figure 6 confirms this, as the black spectrum is fairly similar in size to the magenta spectrum, and both finally feed into the final green spectrum. Therefore, the saturation curve in Figure 5B saturates fast, but not to a high level: it stays a factor of 3−3.5 below the maximum of 50% expected in case of a simple two-level system. Bruggemann and May[36,37] demonstrated for the photosynthetic LH2 antenna ring that upon an 8-fold increase of excitation density the total TA bleaching increased by only on 20%. They used multiexciton density matrix theory to simulate the experimental data with the population of the two-exciton state at $t = 0$, followed by relaxation into the one-exciton after 1 ps. Here, for the PChlide aggregates clearly also exciton theory, but probably including population up to the 3- or even 4-exciton level, is needed to describe the observed spectra and saturation in the aggregate.

We assign the sequential reaction 1 → 2 → 3 → 4 → GS in the target analysis to dynamics of the lowest one-exciton state of the aggregate, whereas states 5 and 6, dominating at high excitation density, we assign to (an average of) higher exciton manifolds. Since the initial population is divided between the two states 1 and 5, both SADS include the contribution from the bleached ground state absorption (GSB), apart from the contributions of stimulated emission (SE) and excited state absorption (ESA) to the relevant levels. In the 1−2−3−4 pathway the SE is due to the transition from the one-exciton state to the GS, therefore it is shifted to the red from the GS bleached absorption peak, whereas the SE in the magenta and cyan spectra of the 5−6−3−4 pathway is due to transitions from the higher exciton manifolds to lower exciton manifolds. In the simplest case, it is the transition from the two-exciton state to the one-exciton state. The GS bleach component corresponds to the area formed by the overlap of the black (or red) and the cyan spectrum in Figure 6. From the decomposition of the cyan SADS (Figure S3, Supporting Information), we can see that while the GS bleach is at 652 nm, the SE peaks at 645 nm, suggesting that the multiexciton SE covers a ~120 cm^{-1} larger energy difference than the GS to one-exciton absorption.

We summarize the scheme of events upon excitation of the Pchlide aggregates in Figure 8. After excitation in the Soret region at 475 nm the system undergoes fast radiationless internal

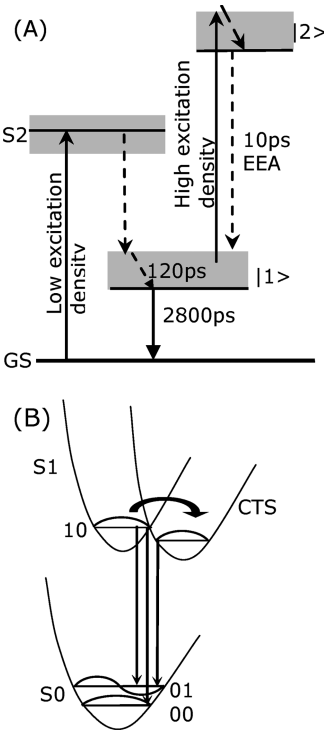

Figure 8. (A) Schematic energy diagram of the aggregated Pchlide in aqueous solution. Dashed arrows indicate a process of radiationless transitions; solid arrows indicate radiative transitions. (B) Mixing of charge-transfer state (CTS) with the S1 state. The transition to a coupled CTS potential leads to a reduced Franck−Condon overlap between the (1−0) excited state and the (0−0) GS levels.

conversion to the one-exciton state $|1\rangle$, on S1. At high excitation density, the aggregate can be promoted to the higher $|2\rangle$-, $|3\rangle$-, or $|4\rangle$-exciton levels. For simplicity, in the diagram only the $|2\rangle$-exciton level is depicted. From the target analysis we find that the population of the high exciton levels decays into the one-exciton manifold with a time constant of 10 ps. This rate is surprisingly slow; in principle, exciton−exciton annihilation should be a determining factor of the $|2\rangle$-, $|3\rangle$-, and $|4\rangle$-exciton state decay. Usually, exciton dynamics are assumed to occur on a subpicosecond time scale,[22,36] as two excitons spatially located within the same domain may be expected to quickly annihilate, transferring their energy to an appropriate resonant monomer vibronic level. In the Pchlide aggregates the intrinsic reactivity of the excited state may be rate-limiting this process. Before we discuss this intrinsic reactivity for the case of the single-exciton dynamics and how it may affect the multiexciton relaxation, we will, however, first turn to a discussion on the structure of the PChlide aggregates.

Structure of Pchlide Water Adduct States. Pchlide is a pigment having a structure very similar to chlorophyll; therefore previous studies of chlorophyll *a* in aqueous solution provide an essential background for understanding the results obtained here. Chlorophyll *a* in wet organic solutions as well as in neat aqueous solution forms aggregates. A chlorophyll dimer or $(Chl-H_2O)_2$ water adduct state is considered to be the basic structural subunit where excitonic interaction is provided via stacking of two conjugated electronic clouds. In addition, chlorophyll *a*−water adduct dimers have been a model for the optical properties of the special pair in PS1 photosynthetic complex, since there is a large resemblance of their visible absorptions. A detailed review of chlorophyll water adduct states and aggregates and various possibilities of mutual chlorophyll and water organization can be found elsewhere.[15,16,38,39] It has been shown that the fundamental and most essential characteristics in such a system is the coordination interaction between a pair of chlorophylls mediated by the OH group of an internal water molecule. Basically, the internal water molecule forms a bridge between the magnesium ion of one chlorophyll and the C═O keto group of another: Mg---H(OH)---O═C. Two water molecules can hold two pigments at a short distance between the macrocycle planes of about 3 Å, close to the optimal van der Waals distance for the porphyrin π-systems. The stacked dimer structure, with overlapping conjugated π-systems, leads to excitonic interaction, causing a red shift in the visible absorption spectrum. In the atomic force microscopy study of the chlorophyll *a* dimer, the internal water molecule was found to be a key element responsible for the formation of chlorophyll a dimers.[29] A 3D structural model of solid self-assembled chlorophyll based on magic angle spinning NMR experiments suggests the presence of structural water molecules that form a hydrogen-bonded network to stabilize chlorophyll sheets.[40]

We suppose that similar to chlorophyll, Pchlide in water forms dimers and oligomers coordinated by strong H-bonding interaction. We estimated the domain size of the aggregates to be 3−4 monomers per complex. It is likely that Pchlide can form dimers in organic solvents like THF as well, resulting in the appearance of a new absorption band at 646 nm (Figure 1C). In this case the red-shifted Q_Y absorption can be due to excitonic coupling provided either by direct stacking of adjacent parallel macrocycles or due to an orthogonally oriented dimer via a Mg---O═C coordination bond. Previously it was shown by quantum chemical calculations[22] that various aggregate structures composed of chlorophyll *a*−dioxane tetramers can be responsible for the appearance of red-shifted Q_Y absorption bands.

The restoration of the emission intensity and the blue shift of the Q_Y band in Pchlide aqueous solution upon addition of THF or pyridine (Figure 1B,C) can now be explained by the ligation of the central magnesium ion by a THF or pyridine molecule, which prevents coordination with a water molecule and breaks the Mg---(OH)---O═C coordinated Pchlide−water adduct states. We also showed that addition of extra OH^- into the Pchlide aqueous solution shifts the position of the Q_Y absorption further to the red (about 2 nm), confirming the correlation between H-bonding, coordination interactions and red shift of the visible absorption. It is likely that the presence of an OH^- ion in the vicinity of the central magnesium and the keto group are crucial factors determining the very complex excited state dynamics in neat water.

Charge Transfer Dynamics in Pchlide Aggregates. In the one-exciton level the dynamics occur on a time scale of 0.5, 5, and 120 ps. From the fluorescence experiments in combination with the transient absorption experiments we conclude that the 0.5 and 5 ps processes represent the formation of a "dark" state with no or low transition dipole moment, since the emission signal is almost totally lost, but the TA signal is only halved, indicating that the ground state absorption is not recovered. Such a dark state could be a state with significant charge-transfer (CT) character: According to a time-dependent density functional theory (TDDFT) study of PChlide,[8] the S1 state is partially of intrinsic CT character. The red shift of monomeric Pchlide emission in the polar protic solvent methanol as observed by Schmitt et al.[5] and later by our group,[6] was ascribed to a dynamic strengthening of the site-specific interaction between polar residues of Pchlide and OH-residues of methanol. Moreover,

strengthening of the H-bonds facilitates the formation of charge-transfer states in the Pchlide excited state in methanol, because electron flow from the solvent to the Pchlide macrocycle and vice versa is coupled to hydrogen bond dynamics.[8] Also individual chlorophylls have electron donor−acceptor properties: The keto C═O group of the cyclopentanone ring V can function as a donor, whereas the central Mg atom serves as an acceptor.[41] Similarly, it was suggested by Zhao and Han[8] that in the electronically excited state of Pchlide, charge can be transferred from the Pchlide macrocycle to the cyclopentanone ring, in particular to the C═O keto group, as well as to the ethylene group at the site of C3. Dietzek et al.[7] suggested an electron withdrawing from the keto group in Pchlide in organic solvents.

The mid-IR absorption difference spectra recorded in the region of the C═O keto stretch mode indeed show significant dynamics, both in the time-dependent position of the bleached bands and in the intensity of the downshifted excited state mode. Interestingly, the time constants are more similar to those of the 1-exciton state, than of the multiexciton state, though the excitation density should have been highly sufficient to excite the multiexciton manifold. Therefore, it appears that the mid-IR spectral changes are more sensitive to the CT-solvation process than to the exciton population dynamics. In the first two fast phases, of 0.6 and 4 ps, the main decay in intensity of the excited state band is observed, which can be identified with the solvation of the CT state. The large intensity of the excited state keto band, probably partially overlapping with the bleached bands, makes an unambiguous interpretation of the dynamics difficult. However, the recovery of high-frequency bleached bands and the bleaching of lower-frequency bands in time can be linked to the observation of the red shift of the transient spectrum in the visible and occurs with similar time constants. It may therefore appear that eventually, either by relaxation from the multiexciton state on the 4−10 ps time scale or by incoherent hopping on the 80−120 ps time scale, the excitation localizes on a population of pigments with strong hydrogen bonds between the C═O groups of Pchlide and the solvent network within and/or surrounding the Pchlide aggregates. Note that a correlation between the strength of hydrogen bonding and a shift of absorption bands toward longer wavelength in the visible region and lower wavenumbers as well in the IR regions has been established.[8,42]

The coordinating internal water molecules, OH---H, possess acidic character due to the high mobility of the proton, making the C═O keto bond more likely to be protonated. The intensity loss of the C═O mode in the excited state (Figure 6) may be the marker of a protonation of the C═O mode. As we argued above, the decay on the 0.5 and 5 ps time scale in the fluorescence and visible transient absorption spectra is caused by loss of stimulated emission due to the formation of a CT state, rather than to a loss of excited states. The decay of the C═O mode can therefore not be explained by excited state decay alone: assuming that the basic structural unit consists of 4 Pchlides, then exciting under saturating conditions should lead to a population of two of these, and to a loss of the initial signal amplitude after annihilation of a factor of 2. Clearly, the decay we see in Figure 6, though difficult to quantify, is significantly more. Generally speaking, the processes of site-specific solvation and protonation of the keto bond in the excited state in Pchlide can be directly related to formation of a state possessing a charge-transfer character.

The possibilities of CTS formation through exciplex mechanism in chlorophyll were discussed earlier,[43] and tautomeric charge-transfer reactions were proposed by Fong[28,44] in the study of chlorophyll water adduct states. Basically, the scheme involves the breaking of the internal coordinating water molecule resulting in ligation of Mg with an OH ion and protonation of the C═O keto group of the other chlorophyll, which can also be considered as the well-known metal-to-ligand/ligand-to-metal charge-transfer state formation mechanism.

From the combination of the time-resolved experiments in the visible and mid-IR, and the considerations discussed above, we conclude that the 0.5 and 5 ps dynamics of Pchlide in water represent sequential solvation processes of the excited/ICT state, which result in strongly coordinated and hydrogen-bonded intermediates, of a strong CT character. We suggest in particular that the 0.5 and 5 ps processes occur in sequence, because the 0.5 ps CT formation may then be competitive with the intrinsic relaxation rate from the multiexciton manifolds, resulting in CT formation on the exciton manifolds.[45] Relaxation to the lower exciton manifolds would then first require the recombination from the CT state, slowing down the relaxation rate to $(10\ \mathrm{ps})^{-1}$. Thus, in the one-exciton state the multiphasic decay of signal, up to ∼120 ps, with the main loss occurring in 0.5 and 5 ps, is due to progressive sequential solvation processes of the excited ICT state that result in a strongly coordinated and hydrogen-bonded intermediates, of strong CT character. For the multiexciton state, decay times of 0.7 and 10 ps are observed. The first time constant we ascribe to the same CT/solvation process as in the 1-exciton state, whereas the second represents the decay from the multi-exciton state into the one-exciton state, limited by charge-recombination occurring in the multiexciton state. Taking into account that we excite into the Soret region, i.e., that also internal conversion (and vibrational relaxation) takes place, we consider the 0.5 and 0.7 ps time constants to be in good agreement with each other. The second phase of solvation is not observed in the multiexciton state, probably the spectral changes associated with recombination-limited decay to the one-exciton state, occurring with a time constant of 10 ps, dominate. Perhaps, higher-quality data would allow for resolving both a 5 ps relaxation process and a 10 ps multi-exciton to one-exciton decay process.

Previously, the excited-state processes in monomeric Pchlide have been studied using time-resolved fluorescence and pump−probe spectroscopy of Pchlide in several organic solvents (methanol, acetonitrile, hexane) in a 360 ps time window.[3,5,46] The complex dynamics were interpreted with a model describing the excited-state processes in terms of a branching of the initially excited-state population into a reactive and a nonreactive path. The reactive path entailed the formation of a state with intramolecular charge-transfer character in 25 ps and subsequent decay in 200 ps; the nonreactive path displayed vibrational relaxation in 4 ps only. More recently we proposed a modification of this sequence of events, based on time-resolved fluorescence and TA experiments performed in the visible and mid-IR:[6] The monomer Pchlide electronic excited state has a nanosecond lifetime, but during the excited state lifetime, the stimulated emission is quenched, due to solvation of the excited state with mixed internal charge-transfer character, into a state with stronger charge-transfer character. This is similar to the current observations, and therefore, apparently Pchlide is an intrinsically reactive molecule in both monomer and aggregated state.

The current findings for PChlide aggregates are relevant for understanding the spectral dynamics in chlorophyll−protein complexes, where the mixing of exciton states with charge-transfer states also occurs: for example, in the red-most chlorophylls in photosynthetic complexes like Photosystem 1,[45,47] and in LHCa1-4

in PS1.[48−50] In addition, we note that there is a striking resemblance between the kinetics found in Pchlide aggregates and those of the Photosystem II core antenna complexes CP43[51] and CP47.[52] In both systems a fast dramatic multiexponential loss of initial signal with time constants of about 1 and 10 ps in CP47, and with time constants of about 200 fs, 3 ps, and 12 ps in CP43, was observed. The final long-lived spectra were found to be red-shifted relatively to the initial spectrum, and there was an enhancement of the blue side of the Q_Y band in the negative TA signals upon an increase of excitation power as well. This may be an indication that also in these pigment−protein complexes population of the multiexciton state occurs and that application of full exciton theory to these (and the current) data, may lead to a better understanding of the excitonic interactions in the antenna complexes.

CONCLUSIONS

Protochlorophyllide (Pchlide) is an important natural porphyrin. The biosynthesis of an entire photosynthetic apparatus in green plants depends on the light-driven redox reaction carried out by the POR enzyme, in which Pchlide is transformed into an immediate precursor of chlorophyll *a*. The dominating form of Pchide in intact etiolated leafs is the 655 nm form, which resembles the red-shifted absorptions of Pchlide in aqueous solutions.

In this work we have studied Pchlide aggregates by ultrafast time-resolved transient absorption and fluorescence experiments in the 480−720 nm visible region and in the 1780−1600 cm^{-1} mid-IR region.

We have shown that Pchlide dissolved in water forms aggregates in which excitonic interactions dominate the optical properties. We have demonstrated the population at high excitation density of multiexciton manifolds, which are characterized by blue-shifted stimulated emission and red-shifted excited state absorption in comparison to those of the one-exciton manifold. The relaxation dynamics of the multiexciton manifolds into the one-exciton manifold occurs in ∼10 ps. We suggest that this rate is slow, because of the formation of a charge-transfer state between the Pchlide molecule and its coordinating water molecule, making the exciton relaxation subject to charge recombination. Support for the charge-transfer process comes form the observed decrease in intensity of the C═O stretch mode in the excited state, concurrent with loss of stimulated emission, on a 0.5 and 5 ps time scale. Finally we note that, to our knowledge, this is the first clear demonstration of the population of multiexciton manifolds ($N > 2$) for an aggregate in solution.

ASSOCIATED CONTENT

Supporting Information. Time-resolved fluorescence traces of Pchlide in H_2O and D_2O. Table of lifetimes for each excitation energy. TA traces. Simulation of double-peaked spectrum. Analysis of saturation curves. This material is available free of charge via the Internet at http://pubs.acs.org.

AUTHOR INFORMATION

Corresponding Author

*E-mail: sytina@amolf.nl.

Notes

†E-mail: I.H.M.v.S., ivo@few.vu.nl; R.v.G., rienk@few.vu.nl; M.L.G., ML.Groot@few.vu.nl.

ACKNOWLEDGMENT

We express their gratitude to The Netherlands Organization for Scientific Research (NWO) for the financial support provided via CW-NWO-TOP grant 700.53.307, and NWO-ALW-Vidi grant 831.00.004. We are thankful to Derren Heyes for providing the purified protochlorophyllide.

REFERENCES

(1) Heyes, D. J.; Hunter, C. N.; van Stokkum, I. H. M.; van Grondelle, R.; Groot, M. L. *Nat. Struct. Biol.* **2003,** *10,* 491.
(2) Sytina, O. A.; Heyes, D. J.; Hunter, C. N.; Alexandre, M. T.; van Stokkum, I. H. M.; van Grondelle, R.; Groot, M. L. *Nature* **2008,** *456,* 1001.
(3) Dietzek, B.; Kiefer, W.; Hermann, G.; Popp, J.; Schmitt, A. *J. Phys. Chem. B* **2006,** *110,* 4399.
(4) Dietzek, B.; Maksimenka, R.; Siebert, T.; Birckner, E.; Kiefer, W.; Popp, J.; Hermann, G.; Schmitt, M. *Chem. Phys. Lett.* **2004,** *397,* 110.
(5) Schmitt, M.; Dietzek, B.; Hermann, G.; Popp, J. *Laser Photon. Rev.* **2007,** *1,* 57.
(6) Sytina, O. A.; van Stokkum, I. H. M.; Heyes, D. J.; Hunter, C. N.; van Grondelle, R.; Groot, M. L. *J. Phys. Chem. B* **2010,** *114,* 4335.
(7) Dietzek, B.; Tschierlei, S.; Hanf, R.; Seidel, S.; Yartsev, A.; Schmitt, M.; Hermann, G.; Popp, J. *Chem. Phys. Lett.* **2010,** *492,* 157.
(8) Zhao, G. J.; Han, K. L. *Biophys. J.* **2008,** *94,* 38.
(9) Heyes, D. J.; Hunter, C. N. *Biochemistry* **2004,** *43,* 8265.
(10) Heyes, D. J.; Martin, G. E. M.; Reid, R. J.; Hunter, C. N.; Wilks, H. M. *FEBS Lett.* **2000,** *483,* 47.
(11) Belyaeva, O. B.; Litvin, F. F. *Biochemistry-Moscow* **2007,** *72,* 1458.
(12) Kobayashi, T. *J-Aggregates*; World Scientific: Singapore, 1996.
(13) Eisfeld, A.; Briggs, J. S. *Chem. Phys.* **2006,** *324,* 376.
(14) Vladkova, R. *Photochem. Photobiol.* **2000,** *71,* 71.
(15) Katz, J. J. *Photosynth. Res.* **1990,** *26,* 143.
(16) Katz, J. J.; Norris, J. R.; Shipman, L. L.; Thurnauer, M. C.; Wasielewski, M. R. *Annu. Rev. Biophys. Bioeng.* **1978,** *7,* 393.
(17) Shipman, L. L.; Cotton, T. M.; Norris, J. R.; Katz, J. J. *Proc. Natl. Acad. Sci. U.S.A.* **1976,** *73,* 1791.
(18) Katz, J. J.; Closs, G. L.; Pennington, F. C.; Thomas, M. R.; Strain, H. H. *Infrared Spectra, Molecular Weights, and Molecular Association of Chlorophylls a and b, Methyl Chlorophyllides, and Pheophytins in Various Solvents* **1963,** *85,* 3801.
(19) Alster, J.; Zupcanova, A.; Vacha, F.; Psencik, J. *Photosynth. Res.* **2008,** *95,* 183.
(20) Savikhin, S.; van Noort, P. I.; Blankenship, R. E.; Struve, W. S. *Biophys. J.* **1995,** *69,* 1100.
(21) Agostiano, A.; Cosma, P.; Trotta, M.; Monsu-Scolaro, L.; Micali, N. *J. Phys. Chem. B* **2002,** *106,* 12820.
(22) Linnanto, J.; Helenius, V. M.; Oksanen, J. A. I.; Peltola, T.; Garaud, J. L.; Korppi-Tommola, J. E. I. *J. Phys. Chem. A* **1998,** *102,* 4337.
(23) Helenius, V. M.; Siikki, J. O.; Hynninen, P. H.; Korppitommola, J. E. I. *Chem. Phys. Lett.* **1994,** *226,* 137.
(24) Helenius, V. M.; Hynninen, P. H.; Korppitommola, J. E. I. *Photochem. Photobiol.* **1993,** *58,* 867.
(25) Groot, M. L.; van Wilderen, L.; Di Donato, M. *Photochem. Photobiol. Sci.* **2007,** *6,* 501.
(26) Kennis, J. T. M.; Groot, M.-L. *Curr. Opin. Struct. Biol.* **2007,** *17,* 623.
(27) van Stokkum, I. H. M.; Gobets, B.; Gensch, T.; van Mourik, F.; Hellingwerf, K. J.; van Grondelle, R.; Kennis, J. T. M. *Photochem. Photobiol.* **2006,** *82,* 380.
(28) Fong, F. K. *Appl. Phys.* **1975,** *6,* 151.
(29) Boussaad, S.; Tazi, A.; Leblanc, R. M. *Proc. Natl. Acad. Sci. U.S.A.* **1997,** *94,* 3504.
(30) Mylsiwa-Kurdziel, B.; Kruk, J.; Strzalka, K. *Photochem. Photobiol.* **2004,** *79,* 62.
(31) van Stokkum, I. H. M.; Larsen, D. S.; van Grondelle, R. *Biochim. Biophys. Acta—Bioenerg.* **2004,** *1657,* 82.
(32) Sytina, O. A.; van Stokkum, I. H. M.; Heyes, D. J.; Hunter, C. N.; van Grondelle, R.; Groot, M. L. *J. Phys. Chem. B* , *114,* 4335.

(33) Groot, M.-L.; van Grondelle, R.; Leegwater, J.-A.; van Mourik, F. *J. Phys. Chem. B* **1997,** *101,* 7869.
(34) Sytina, O. A.; Alexandre, M. T.; Heyes, D. J.; Hunter, C. N.; Robert, B.; van Grondelle, R.; Groot, M. L. *Phys. Chem. Chem. Phys.,* DOI: 10.1039/C0CP01686A.
(35) Stiel, H.; Leupold, D.; Teuchner, K.; Nowak, F.; Scheer, H.; Cogdell, R. J. *Chem. Phys. Lett.* **1997,** *276,* 62.
(36) Bruggemann, B.; May, V. *J. Chem. Phys.* **2004,** *120,* 2325.
(37) Bruggemann, B.; Sznee, K.; Novoderezhkin, V.; van Grondelle, R.; May, V. *J. Phys. Chem. B* **2004,** *108,* 13536.
(38) Strouse, C. E. *Proc. Natl. Acad. Sci. U.S.A.* **1974,** *71,* 325.
(39) Katz, J. J. *Naturwissenschaften* **1973,** *60,* 32.
(40) van Rossum, B. J.; Schulten, E. A. M.; Raap, J.; Oschkinat, H.; de Groot, H. J. M. *J. Magn. Reson.* **2002,** *155,* 1.
(41) Sidorov, A. N. *Russ. Chem. Rev.* **1966,** *35,* 152.
(42) Rozenberg, M.; Loewenschuss, A.; Marcus, Y. *Phys. Chem. Chem. Phys.* **2000,** *2,* 2699.
(43) Hindman, J. C.; Kugel, R.; Wasielewski, M. R.; Katz, J. J. *Proc. Natl. Acad. Sci. U.S.A.* **1978,** *75,* 2076.
(44) Fong, F. K. *Proc. Natl. Acad. Sci. U.S.A.* **1974,** *71,* 3692.
(45) Novoderezhkin, V. I.; Dekker, J. P.; van Grondelle, R. *Biophys. J.* **2007,** *93,* 1293.
(46) Dietzek, B.; Tschierlei, S.; Hermann, G.; Yartsev, A.; Pascher, T.; Sundstrom, V.; Schmitt, M.; Popp, J. *Chemphyschem* **2009,** *10,* 144.
(47) Vaitekonis, S.; Trinkunas, G.; Valkunas, L. *Photosynth. Res.* **2005,** *86,* 185.
(48) Croce, R.; Chojnicka, A.; Morosinotto, T.; Ihalainen, J. A.; van Mourik, F.; Dekker, J. P.; Bassi, R.; van Grondelle, R. *Biophys. J.* **2007,** *93,* 2418.
(49) Frese, R. N.; Palacios, M. A.; Azzizi, A.; van Stokkum, I. H. M.; Kruip, J.; Rögner, M.; Karapetyan, N. V.; Schlodder, E.; van Grondelle, R.; Dekker, J. P. *Biochim. Biophys. Acta—Bioenerg.* **2002,** *1554,* 180.
(50) Romero, E.; Mozzo, M.; van Stokkum, I. H. M.; Dekker, J. P.; van Grondelle, R.; Croce, R. *Biophys. J.* **2009,** *96,* L35.
(51) Di Donato, M.; van Grondelle, R.; van Stokkum, I. H. M.; Groot, M. L. *J. Phys. Chem. B* **2007,** *111,* 7345.
(52) Groot, M. L.; Breton, J.; van Wilderen, L. J. G. W.; Dekker, J. P.; van Grondelle, R. *J. Phys. Chem. B* **2004,** *108,* 8001.